JOURNAL OF MATERIALS SCIENCE 28 (1993) 5099–5111

A critical evaluation of theories for predicting microcracking in composite laminates

JOHN. A. NAIRN, SHOUFENG HU, JONG SEOK BARK
Material Science and Engineering, University of Utah, Salt Lake City, Utah 84112, USA

We present experimental results on 21 different layups of Hercules AS4 carbon fibre/3501-6 epoxy laminates. All laminates had 90° plies; some had them in the middle ($[(S)/90_n]_s$) while some had them on a free surface ($[90_n/(S)]_s$). The supporting sublaminates, (S), where $[0_n]$, $[\pm 15]$, or $[\pm 30]$. During tensile loading, the first form of damage in all laminates was microcracking of the 90° plies. For each laminate we recorded both the crack density and the complete distribution of crack spacings as a function of the applied load. By rearranging various microcracking theories we developed a master-curve approach that permitted plotting the results from all laminates on a single plot. By comparing master-curve plots for different theories it was possible to critically evaluate the quality of those theories. We found that a critical-energy-release-rate criterion calculated using a two-dimensional variational stress analysis gave the best results. All microcracking theories based on a strength-failure criteria gave poor results. All microcracking theories using one-dimensional stress analyses, regardless of the failure criterion, also gave poor results.

1. Introduction

When the 90° plies are relatively less stiff than the supporting plies, the first form of damage in $[(S)/90_n]_s$ or $[90_n/(S)]_s$ laminates (where (S) denotes any orthotropic sublaminate) is usually microcracking or transverse cracking of the 90°-ply groups [1–24]. When the 90° plies are in the middle ($[(S)/90_n]_s$ laminates), those plies crack into an array of roughly periodic microcracks. When the 90° plies are on the outside ($[90_n/(S)]_s$ laminates), the 90°-ply groups also crack into an array of roughly periodic microcracks, but the two arrays are shifted from each other by half the average crack spacing [11, 25]. Typical damage states for $[(S)/90_n]_s$ and $[90_n/(S)]_s$ laminates are shown in Fig. 1.

There are many reasons for studying microcracking. Microcracks not only change the thermal and mechanical properties of laminates [11, 26, 27], but they also present pathways through which corrosive agents may penetrate into the interior of the laminate [6]. Perhaps most importantly, microcracks act as nuclei for further damage such as delamination [1, 10, 14, 28], longitudinal splitting [5, 6], and curved microcracks [21, 29]. Because microcracks are precursors to the cascade of events that leads to laminate failure, we would have little hope of understanding laminate failure or of predicting long-term durability if we did not first develop a thorough understanding of the phenomenon of microcracking. To understand microcracking, we must be able to predict the initiation of microcracking, the increase in microcrack density with increasing load, the conditions under which microcracks nucleate other forms of damage, the differences between $[(S)/90_n]_s$ and $[90_n/(S)]_s$ laminates, and the effect of residual thermal stresses [30]. A successful microcracking analysis should be fundamental and should not resort to empiricism. A typical empirical analysis introduces *in situ* parameters such as layup-dependent ply strengths. The use of such parameters destroys the useful predictive capabilities of an analysis.

Because of the importance of understanding microcracking, there has been much work in the past 15 years aimed at explaining and predicting experimental observations. The first step towards understanding microcracking is to consider the effect of microcracks on the stresses and strains in the laminate. Most microcracking stress analyses are one-dimensional [1, 2, 5, 12, 31–39]. For the reasons given below, we refer to any analysis that ignores the through-the-thickness stresses as a one-dimensional analysis. Hashin used variational mechanics to develop the first two-dimensional analysis of the stresses in microcracked $[(0_m)/90_n]_s$ laminates [40, 41]. Nairn *et al.* extended Hashin's results to include residual thermal stresses [23, 42], to handle the more general $[(S)/90_n]_s$ laminates [28], and to analyse laminates with surface 90° plies ($[90_n/(S)]_s$ laminates) [25]. The second step towards understanding microcracking is to propose a failure criterion and use some calculated stress state to predict experimental results. Some workers have proposed strength models which claim that a microcrack forms when the longitudinal stress in the 90° plies reaches the transverse strength of those plies [1, 4, 12, 13, 22, 34, 43]. More recent work has proposed energy models which claim that a microcrack forms when the energy-release rate reaches a critical value [3, 5, 17, 20, 23, 25, 30, 35–37, 39, 42].

0022–2461

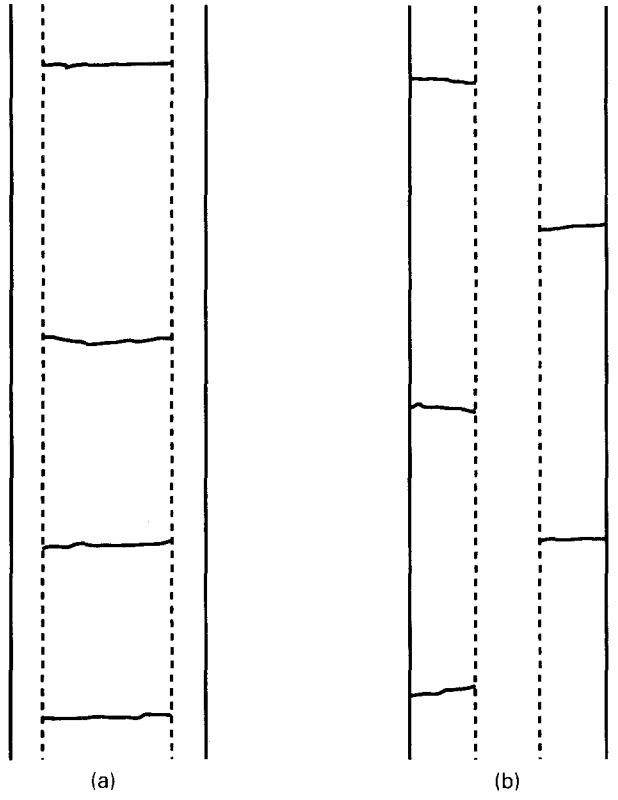

Figure 1 Sketches of the actual damage in cross-ply laminates. (a) Roughly periodic array of microcracks in a $[0/90_4]_s$ laminate. (b) Antisymmetric or staggered microcracks in a $[90_4/0_2]_s$ laminate.

There are numerous opinions regarding the most appropriate method for predicting the microcracking properties of composites. To provide a critical test for microcracking theories, we measured the crack density as a function of applied load for 21 different layups of Hercules AS4 carbon fibre/3501-6 epoxy composites. The range of laminates included $[(S)/90_n]_s$ and $[90_n/(S)]_s$ laminates. The supporting sublaminates (S) included $[0_n]$, $[\pm 15]$, and $[\pm 30]$ sublaminates. A *fundamental* microcracking analysis should be able to take a single material property, such as transverse ply strength or intralaminar fracture toughness, and predict the results for all 21 laminates. To facilitate the comparison of various microcracking theories, we developed a master-curve method. In brief, the various stress analyses were used to develop scaling laws that permit plotting the results from all laminates on a single, linear, master plot. The accuracy with which any analysis conforms to the linear, master-plot predictions quickly reveals the adequacy of that analysis. Our findings were that the only satisfactory analysis is one that uses two-dimensional, variational-stress analysis with an energy-release-rate failure criterion. All theories that rely on one-dimensional stress analyses gave poor results.

2. Materials and methods

Static tensile tests were run on Hercules AS4 carbon fibre/3501-6 epoxy-matrix composites. The material was purchased from Hercules in prepreg form and cured in an autoclave at 177 °C according to the manufacturer's recommendations. We made eight cross-ply layups with 90° plies in the middle – $[0/90]_s$, $[0/90_2]_s$, $[0/90_4]_s$, $[0_2/90]_s$, $[0_2/90_2]_s$, $[0_2/90_4]_s$, $[\pm 15/90_2]_s$, and $[\pm 30/90_2]_s$. We made 13 cross-ply layups with surface 90° plies – $[90/0/90]_T$, $[90/0]_s$, $[90/0_2]_s$, $[90/0_4]_s$, $[90_2/0/90_2]_T$, $[90_2/0]_s$, $[90_2/0_2]_s$, $[90_2/0_4]_s$, $[90_2/\pm 15]_s$, $[90_2/\pm 30]_s$, $[90_3/0]_s$, $[90_3/0_2]_s$ and $[90_4/0_2]_s$. Specimens, which were nominally 12 mm wide and 150 mm long with thicknesses determined by the stacking sequences (about 0.125 mm per ply), were cut from the cured laminates. All specimens had 19 mm by 12 mm aluminium end tabs attached using Hysol 9230 epoxy.

All tensile tests were run in displacement control, at a rate of 0.005 mm s^{-1}, on a Minnesota Testing Systems (MTS) 25 kN servohydraulic testing frame. Load–displacement curves were collected on an IBM PC-XT that was interfaced to an MTS 464 Data Display Device. While testing each specimen, the experiment was periodically stopped and the specimen was examined by optical microscopy. For $[(S)/90_n]_s$ laminates we mapped the complete distribution of microcrack spacings on either edge of the specimen. To get an average crack density, we averaged the densities on the two specimen edges. For $[90_n/(S)]_s$ laminates, microcracks could be seen on the edges and on the faces of the specimen. We mapped the complete distribution of microcrack spacings in each of the two surface 90°-ply groups. To get an average crack density, we averaged the densities of the two 90°-ply groups. The specimens were continually reloaded into the MTS frame and tested to higher displacements until the end tabs failed, the specimen broke, or delamination began.

3. Experimental observations

To provide a critical test of microcracking theories we tested 21 different layups of AS4/3501-6 laminates. Eight of the tested laminates had 90° plies in the middle. Many previous investigators have reported results for such $[(S)/90_n]_s$ laminates [1–24]. The results for our tests agreed with previous experimental observations except that we have the largest number of layups for a single material ever included in a single study. The $[(S)/90_n]_s$ laminates all developed a roughly periodic array of microcracks in the 90° plies (see Fig. 1a). The microcracks stopped at the $(S)/90$ interface with little tendency to cause delamination until the crack density and applied strain became sufficiently high. The first microcrack occurred at lower strains for laminates with thicker 90°-ply groups. In contrast, the maximum crack density observed at high strains was larger for laminates with thinner 90°-ply groups. The microcrack density as a function of applied load for these laminates is discussed in Section 4. The reader is referred to [23] for typical, raw plots of crack density against applied load for $[(S)/90_n]_s$ laminates.

The microcracking properties of $[90_n/(S)]_s$ laminates are much less commonly studied (see [5, 8, 11, 22]). Thirteen of our tested laminates had 90° plies on the free surfaces – the $[90_n/(S)]_s$ laminates. They all developed a roughly periodic array of microcracks in

each of the surface 90-ply groups. As shown in Fig. 1b, the microcracks in one 90°-ply group were systematically staggered from the microcracks in the other 90°-ply group. Some typical, raw plots of crack density against applied load for $[90_n/(S)]_s$ laminates are shown in Fig. 2. As in $[(S)/90_n]_s$ laminates, the first microcrack occurred at lower strains for laminates with thicker 90°-ply groups. The absolute value of the microcrack initiation strain, however, was lower for $[90_n/(S)]_s$ laminates than it was for the companion $[(S)/90_n]_s$ laminates. This general trend was sometimes obscured by scatter at low crack densities that could be attributed to laminate-processing flaws [23]. At high crack densities, the damage state in $[90_n/(S)]_s$ laminates had a lower crack density than the damage state in the companion $[(S)/90_n]_s$ laminates. The differences were significant – typically a factor of two. Although early microcracks stopped at the (S)/90 interface, $[90_n/(S)]_s$ laminates had a greater tendency to delaminate than $[(S)/90_n]_s$ laminates. The tendency towards delamination increased as the thickness of the 90° plies increased. These qualitative delamination observations agree with stress-analysis predictions in [25]. In the three laminates with the thickest 90°-ply groups, $[90_3/0]_s$, $[90_3/0_2]_s$, and $[90_4/0_2]_s$, delamination started soon after the first microcrack. Because we could not obtain sufficient microcrack-density data for these laminates, they were ignored in the microcracking analyses described in Section 4.

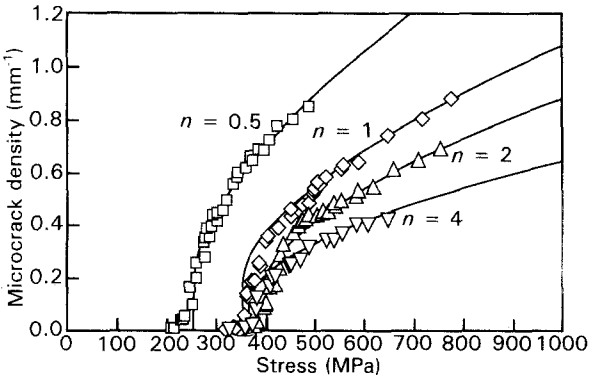

Figure 2 Microcrack density as a function of applied load in a series of AS4/Hercules 3501-6 carbon/epoxy laminates ($[90/0_n]_s$). The symbols are experimental data points. The smooth lines are predictions using variational-mechanics-energy-release-rate theory and $G_{mc} = 240\ J\,m^{-2}$.

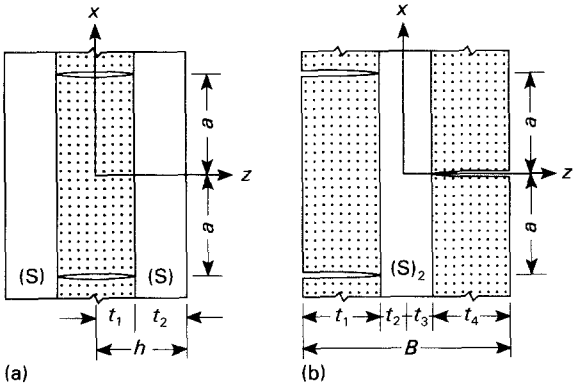

Figure 3 Edge views of microcracks in the 90° plies of laminates. (a) Two microcracks in a $[(S)/90_n]_s$ laminate. (b) Three staggered microcracks in a $[90_n/(S)]_s$ laminate.

4. Analysis results

4.1. $[(S)/90_n]_s$ laminates: Energy-release-rate analysis

We first consider $[(S)/90_n]_s$ laminates under an axial stress, σ_0, in the x-direction. Under most experimental conditions, the microcracks that form in the 90° plies span the entire cross-section of those plies as through-the-width cracks [30]. In the presence of only through-the-width damage, the stress analysis is approximately two-dimensional in the (x, z)-plane or the laminate-edge plane. The co-ordinate system for the stress analysis is shown in Fig. 3a. Hashin used variational mechanics to derive the first two-dimensional, analytical stress analysis for the (x, z)-plane of a microcracked $[0_m/90_n]_s$ laminate [40, 41]. His only assumption is that the x-axis normal stresses in the 0° and the 90° plies are functions of x, but are independent of z. He determines the best approximate stress state, under his one assumption, by minimizing the total complementary energy. Nairn and co-workers extended Hashin's analysis to include residual thermal stresses and to handle general $[(S)/90_n]_s$ laminates [23, 28, 42].

The variational-mechanics analysis determines all components of the stress tensor in the (x, z)-plane. In this paper, we only require the tensile stress in the 90° plies. The result from [23] is

$$\sigma_{xx}^{(1)}(\xi) = \sigma_{x0}^{(1)}[1 - \phi(\xi)] \quad (1)$$

where the superscript (1) denotes the 90° plies, $\sigma_{x0}^{(1)}$ is the tensile stress in the 90° plies in the absence of microcracking damage, and $\phi(\xi)$ is a perturbation function determined by the variational analysis (see the Appendix). Equation 1 and all subsequent equations are written in terms of a dimensionless x-direction co-ordinate defined as

$$\xi = \frac{x}{t_1} \quad (2)$$

where t_1 is the semi-thickness of the 90° ply group. For a linear thermoelastic material we can write

$$\sigma_{x0}^{(1)} = k_m^{(1)}\sigma_0 + k_{th}^{(1)}T \quad (3)$$

where σ_0 is the total applied axial stress and $T = T_s - T_0$ is the difference between the specimen temperature, T_s, and the effective stress-free temperature, T_0. (Note that [23, 25, 28, 40, 41, 42] define $\sigma_{x0}^{(1)} = k_m^{(1)}\sigma_0$ or as the mechanical load in 90° plies of the undamaged laminate. As expressed in Equation 3, we altered the definition of $\sigma_{x0}^{(1)}$ to also include the initial thermal stresses.) The terms $k_m^{(1)}$ and $k_{th}^{(1)}$ are the effective thermal and mechanical stiffnesses of the 90° plies. By a simple one-dimensional, constant-strain analysis they are

$$k_m^{(1)} = \frac{E_x^{(1)}}{E_c^0}, \quad k_{th}^{(1)} = -\frac{\Delta\alpha}{C_1} \quad (4)$$

Here E_c^0 is the x-direction modulus of the laminate, $E_x^{(1)}$ is the x-direction modulus of the 90° plies,

$\Delta\alpha = \alpha_x^{(1)} - \alpha_x^{(2)}$ is the difference between the x-direction thermal-expansion coefficients of the 90° plies and the (S) sublaminate, and C_1 is a constant defined in the Appendix. Alternatively, $k_m^{(1)}$ and $k_{th}^{(1)}$ could be found by a laminated-plate-theory analysis of the undamaged laminate. The results, however, would only differ from Equation 4 by 2 to 5% [30].

To predict microcracking results, Liu and Nairn [23, 42] advocated an energy-release-rate failure criterion. In brief, the next microcrack is assumed to form when the total energy-release rate associated with the formation of that microcrack, G_m, equals or exceeds the microcracking fracture toughness of the material, G_{mc}. From the thermoelastic, variational-mechanics stress state, the total energy-release rate from [23] and [42] is

$$G_m = (\sigma_{x0}^{(1)})^2 C_3 t_1 Y(D) \quad (5)$$

where C_3 is a constant defined in the appendix and

$$Y(D) = LW \frac{d}{dA} \frac{\sum_{i=1}^{N} \chi(\rho_i)}{\sum_{i=1}^{N} \rho_i} = \frac{d}{dD}(D\langle\chi(\rho)\rangle) \quad (6)$$

In Equation 6, $\chi(\rho)$ is a function determined by the variational analysis (see the Appendix), and the summation refers to a sample with N microcrack intervals having aspect ratios (a_i/t_1) of $\rho_1, \rho_2, \ldots, \rho_N$. $A = 2t_1 LWD$ is the total microcrack surface area, $D = (2\langle\rho\rangle t_1)^{-1}$ is the average crack density, L is the sample length, and W is the sample width. The angular bracket notation implies an average of that quantity over the N microcrack intervals.

To use Equation 5, $Y(D)$ is needed. Following Laws and Dvorak [37], Liu and Nairn [23, 42] evaluated $Y(D)$ for the discrete process of forming a new microcrack at the dimensionless position $\xi = 2\delta - \rho_k$ in the kth microcrack interval. The result is

$$Y(D) = \frac{\Delta D\langle\chi(\rho)\rangle}{\Delta D} = \chi(\rho_k - \delta) + \chi(\delta) - \chi(\rho_k) \quad (7)$$

Without tedious and perhaps impossible observation tasks one does not know where the next microcrack will form and therefore ρ_k and δ are not known. It is known, however, that $[(S)/90_n]_s$ laminates tend to form roughly periodic microcracks. We thus might expect $\rho_k \approx \langle\rho\rangle$ and $\delta \approx \langle\rho\rangle/2$. Liu and Nairn [23], however, point out that these approximations are an oversimplification. From Equation 5 it can be shown that the energy release rate is higher when the microcrack forms in a large microcrack interval than it is when it forms in a small microcrack interval. It is logical to assume that microcrack formation is preferred in the location that maximizes the energy-release rate. Thus, when there is a distribution in crack spacings, the next microcrack will form preferably in a crack interval that is larger than the average crack spacing. Liu and Nairn [23] introduced a factor, f, defined as the average ratio of the crack spacing, where the new microcrack forms, to the average crack spacing. In this model, $Y(D)$ is approximated by

$$Y(D) \approx 2\chi(f\langle\rho\rangle/2) - \chi(f\langle\rho\rangle) \quad (8)$$

The f-factor can be treated as an adjustable parameter when fitting microcracking results to Equation 5. Using f-values between 1.0 and 1.44, Liu and Nairn [23] found good fits to experimental results for a wide variety of laminates. Fortunately, the value of f selected to get the best fit does not influence the calculated fracture toughness, G_{mc}. In this section, we treat f as a layup-independent factor that is approximately 1.2. In a later section we describe a tedious experimental procedure to measure f.

Solving Equation 5 for a given material we get

$$\sigma_0 = \frac{1}{k_m^{(1)}}\left[\left(\frac{G_{mc}}{C_3 t_1 Y(D)}\right)^{1/2} - k_{th}^{(1)} T\right] \quad (9)$$

There are three unknowns in Equation 9: G_{mc} or the microcracking fracture toughness, T or the temperature difference that determines the level of residual thermal stresses, and f in the definition of $Y(D)$. T can be measured by various means, or when it is not available it can be estimated from knowledge of the processing conditions. For AS4/3501-6 laminates we estimated $T = -125\,°C$ [23]. When f is not measured it can be assumed to be approximately 1.2. We are left with one unknown: G_{mc}. If Equation 9 provides a *fundamental* analysis of microcracking, it should be possible to predict the experimental results for all $[(S)/90_n]_s$ laminates using a single value of G_{mc}.

We applied Equation 9 to the eight $[(S)/90_n]_s$ laminates tested in this study. We found that all eight could be fitted with $G_{mc} = 280\,J\,m^{-2}$. This paper focuses on the master-curve analysis of these laminates. The reader is therefore referred to [23] and [30] for typical fits of Equation 9 to the raw experimental data of microcrack density plotted against applied stress. All eight fits were found to be good. The only discrepancies appeared at low crack density. These were attributed to laminate flaws that are not explicitly included in the analysis [23, 30]. The newly determined value of G_{mc} agrees well with results for this material previously measured by Liu and Nairn [23] ($G_{mc} = 240\,J\,m^{-2}$) and by Yalvac *et al.* [24] ($G_{mc} = 230\,J\,m^{-2}$).

4.2. $[90_n/(S)]_s$ laminates: Energy-release-rate analysis

The variational analysis of $[90_n/(S)]_s$ laminates is more complicated due to the loss of symmetry resulting from staggered microcracks. Nairn and Hu [25] extended Hashin's analysis [40, 41] to the staggered microcracking pattern shown in Fig. 3b. Their results can be cast in a form similar to the $[(S)/90_n]_s$ laminate results. The tensile stress in the 90° plies on the left-hand side of Fig. 3b is

$$\sigma_{xx}^{(1)}(\xi) = \sigma_{x0}^{(1)}(1 - \phi_a(\xi)) \quad (10)$$

where $\phi_a(\xi)$ is a new function determined by variational analysis (see the Appendix). The subscript "a" denotes antisymmetric damage. Likewise, the total-strain-energy release rate associated with an increase in microcracking damage is

$$G_m = (\sigma_{x0}^{(1)})^2 C_{3a} t_1 Y_a(D) \quad (11)$$

where C_{3a} is a constant defined in the Appendix and

$$Y_a(D) = LW\frac{d}{dA}\frac{\sum_{i=1}^{N}\chi_a(\rho_i)}{\sum_{i=1}^{N}\rho_i} = \frac{d}{dD}(D\langle\chi_a(\rho)\rangle) \quad (12)$$

In Equation 12, the function $\chi_a(\rho)$, which is determined by variational analysis (see the Appendix), is the antisymmetric-damage-state analog of $\chi(\rho)$. Accounting for the staggered crack geometry and using the same approximations that were successful for $[(S)/90_n]_s$ laminates, $Y_a(D)$ can be approximated by [25]

$$Y_a(D) \approx \tfrac{1}{2}(3\chi_a(f\langle\rho\rangle/3) - \chi_a(f\langle\rho\rangle)) \quad (13)$$

Equation 9, with $Y(D)$ replaced by $Y_a(D)$, is the prediction for crack density as a function of applied stress for $[90_n/(S)]_s$ laminates. To test the predictions, we compared the experimental results for the ten laminates with sufficient microcracking data, to the theoretical predictions. In fact, we have a more rigorous test of the analysis for $[90_n/(S)]_s$ laminates than for $[(S)/90_n]_s$ laminates, because the results on $[(S)/90_n]_s$ laminates can be viewed as experiments that measured $G_{mc} = 280\ J\,m^{-2}$. If Equation 11 correctly accounts for outer-ply 90° plies with staggered microcracks, then it should be possible to fit experimental results for $[90_n/(S)]_s$ laminates with the same value of G_{mc}. Because results for crack density versus applied stress for $[90_n/(S)]_s$ laminates have rarely appeared in the literature, we give one plot of the comparison between theory and experiment in Fig. 2. The results in Fig. 2 are for $[90/0_n]_s$ laminates with $n = 0.5$, 1, 2, and 4; they are analysed with the assumptions that $T = -125\,°C$ and $f \approx 1.2$. All results are well fitted by a single value of $G_{mc} = 240\ J\,m^{-2}$. This microcracking fracture toughness is lower than the toughness used to fit the results for $[(S)/90_n]_s$ but close enough to be within experimental uncertainty. It is in better agreement with the results of Liu and Nairn [23] and Yalvac *et al.* [24]. In general, fits for $[90_n/(S)]_s$ laminates are slightly better than fits for $[(S)/90_n]_s$ laminates.

4.3. Master-curve analysis

Multiplying Equation 9 by $-k_m^{(1)}/k_{th}^{(1)}$ gives

$$-\frac{k_m^{(1)}}{k_{th}^{(1)}}\sigma_0 = -\frac{1}{k_{th}^{(1)}}\left(\frac{G_{mc}}{C_3 t_1 Y(D)}\right)^{1/2} + T \quad (14)$$

This equation leads us to define a reduced stress and a reduced crack density, respectively, as

$$\sigma_R = -\frac{k_m^{(1)}}{k_{th}^{(1)}}\sigma_0$$

$$D_R = -\frac{1}{k_{th}^{(1)}}\left(\frac{1}{C_3 t_1 Y(D)}\right)^{1/2} \quad (15)$$

A plot of σ_R against D_R defines a master curve for microcracking experiments. If the variational analysis and energy-release-rate failure criterion are appropriate, a plot of σ_R against D_R will be linear with slope $(G_{mc})^{1/2}$ and intercept T. Because G_{mc} and T are layup-independent material properties, the results from all laminates of a single material with the same processing conditions should fall on the same linear master curve. A critical test of the variational-analysis microcracking theory is to determine if the master curve is linear and if all laminates fall on the same line. Furthermore, the resulting slope and intercept should define physically reasonable quantities.

A typical master-curve analysis for a single $[90_2/0_2]_s$ laminate is shown in Fig. 4. The master plot is linear except for a few points at the lowest crack density. As previously discussed, the low-crack-density results are affected by processing flaws that are not specifically included in the microcracking analysis [23]. It is not surprising that they deviate from the master curve, and they should be ignored when measuring G_{mc}. The straight line in Fig. 4 is the best linear fit that ignores the low-crack-density data. The slope gives $G_{mc} = 264\ J\,m^{-2}$, which agrees with the fits to raw data in Section 3 and with the results in other studies [23, 24]. The intercept gives $T = -93\,°C$, which is reasonable and is similar to the previously assumed value of $T = -125\,°C$ [23]. Note that a side benefit of the master-curve analysis is that the value of T does not have to be assumed or measured. It can, in effect, be measured by analysis of the microcracking data. We comment more on measuring T in Section 5.

Figure 5 gives the master curve for the 18 laminates tested in this study. We assumed that $f = 1.2$ for all laminates and we ignored data with crack densities less than $0.3\ mm^{-1}$. We claim Fig. 5 verifies both the validity of an energy-release-rate failure criterion and the accuracy of the variational-analysis calculation of G_m in Equations 5 and 11. Three facts support this claim. First, all laminates fall on a single master-curve plot within a relatively narrow scatter band. We discuss the scatter below. Secondly, the results for $[(S)/90_n]_s$ laminates (□) agree with the results for the $[90_n/(S)]_s$ laminates (■). Thus a single unified analysis can account for both the symmetric damage state in $[(S)/90_n]_s$ laminates and the antisymmetric damage state in $[90_n/(S)]_s$ laminates. Thirdly, the slope and the intercept of the global linear fit in Fig. 5 result in $G_{mc} = 279\ J\,m^{-2}$ and $T = -93\,°C$. Both of these results are reasonable measured values for these physical quantities.

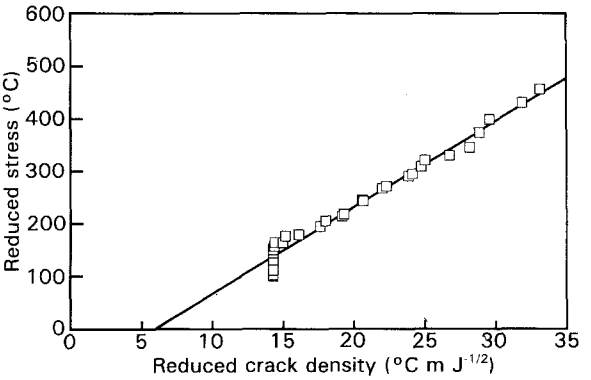

Figure 4 A master-curve analysis (stresses: variational analysis) of a $[90_2/0_2]_s$ AS4/3501-6 laminate. The energy-release rate is calculated with a discrete energy derivative defined by $Y_a(D)$ in Equation 13 using $G_{mc} = 264\ J\,m^{-2}$, $\Delta T = -97\,°C$ and $f = 1.2$.

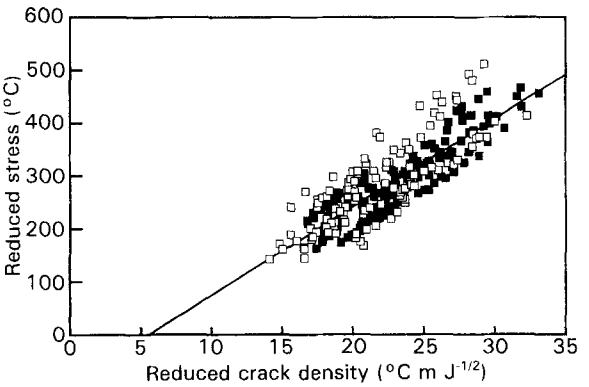

Figure 5 A master-curve analysis of all AS4/3501-6 laminates: (□) $[0_n/90_m]_s$ and (■) $[90_n/0_m]_s$. The energy-release rate is calculated with a discrete energy derivative defined by $Y(D)$ or $Y_a(D)$ in Equations 8 and 13 using $f = 1.2$. Data for crack densities less than 0.3 mm^{-1} are not included in this plot.

There is an observable scatter band for the experimental points relative to the global, linear, master curve. This scatter band may represent deficiencies in the analysis that need further refinement. Alternatively, we note that the scatter was caused more by a laminate-to-laminate variation in the intercept than by a laminate-to-laminate variation in the slope. It is thus possible that the scatter is due to real variations in T. Physically, $T = T_s - T_0$, and because all laminates were processed under identical conditions T should be the same for all laminates. T, however, can also be interpreted as the *effective* level of residual thermal stresses. By Equation 3, when $\sigma_0 = 0$ the residual stress in the 90° plies is $\sigma^{(1)}_{xx,\,th} = k^{(1)}_{th} T$. Although all laminates were processed under identical conditions, the laminates had different thicknesses. If the different thicknesses caused variations in thermal history, it is possible that the level of residual stresses was layup dependent. A layup dependence in T would cause the type of scatter observed in Fig. 5.

4.4. Master-curve analysis for other microcracking theories

Most previous microcracking theories are based on stress analyses that eliminate the z-dependence of the stress state by making various assumptions about the z-direction stress or displacement. The common assumptions are zero stress, zero average stress, or zero displacement. We classify any analysis using one of these assumptions as a "one-dimensional" analysis. Examples can be found in Refs. [1, 2, 5, 12, 31–39]. We note that some authors describe their analyses as "two-dimensional" analyses [33, 34, 38, 39]. In all cases, however, the second dimension is the y-dimension, whose inclusion is little more than a correction for Poisson's contraction. The difference between a two-dimensional (x, y)-plane analysis and a one-dimensional, x-axis analysis is marginal [30].

The first one-dimensional analysis is described by Garrett and Bailey [1]. They used a shear-lag approximation to derive a second-order differential equation for the total stress transferred from the 90° plies to the (S) sublaminate, $\Delta\sigma$, defined as

$$\Delta\sigma(x) = \langle\sigma^{(2)}_{xx}(x)\rangle - \sigma^{(2)}_{x0} \tag{16}$$

By using a consistent nomenclature and transposing all equations to the dimensionless ξ-coordinate, we find that all one-dimensional analyses [1, 2, 5, 12, 31, 32, 35–37] (including the "two-dimensional" (x, y)-plane analyses [33, 34, 38, 39]) can be reduced to a generalized form of Garrett and Bailey's equation [1]:

$$\frac{d^2\Delta\sigma}{d\xi^2} - \Phi^2\Delta\sigma = \omega(P) \tag{17}$$

where Φ is a constant which depends on laminate properties and material properties, and $\omega(P)$ is a function of the applied load. The boundary conditions for Equation 17 are

$$\Delta\sigma(\pm\rho) = \frac{t_2\sigma^{(1)}_{x0}}{t_1} \tag{18}$$

The constant Φ governs the rate of stress transfer by shear at the 90/(S) interface and we call it the shear-stress transfer coefficient. The function $\omega(P)$ is zero in all analyses except that of Nuismer and Tan [38, 39]. It has little effect on the predictions [30] and we set $\omega(P) = 0$ in subsequent calculations.

Equation 17 can be solved easily. The tensile stress in the 90° plies is identical to Equation 1 except that $\phi(\xi)$ is redefined as

$$\phi_{1D}(\xi) = \frac{\cosh\Phi\xi}{\cosh\Phi\rho} \tag{19}$$

The tensile stress in the sublaminate (S) and the shear stresses can be found from Equation 19 by force balance and stress equilibrium. The z-direction normal stresses are undefined in all one-dimensional analyses. From these stress results, it is possible to propose failure criteria and to make predictions about microcracking. In this section we examine the results of several previous one-dimensional microcracking theories.

Garrett and Bailey [1] postulated that the next microcrack forms when the maximum stress in the 90° plies, which occurs at $\xi = 0$, reaches the transverse strength of those plies. By this failure criterion, Equations 1 and 19 can be rearranged to give a strength-theory master curve

$$-\frac{k^{(1)}_m}{k^{(1)}_{th}}\sigma_0 = -\frac{1}{k^{(1)}_{th}}\frac{\sigma_T}{[1 - \phi_{1D}(0)]} + T \tag{20}$$

where σ_T is the transverse strength of the 90° plies and, as calculated by Garrett and Bailey [1], $\Phi = (G^{(1)}_{xx}C_1)^{1/2}$. Defining the reduced stress as in Equation 15 and the reduced crack density as

$$D_R = -\frac{1}{k^{(1)}_{th}}\frac{1}{(1 - \phi_{1D}(0))} \tag{21}$$

and using a master-curve analysis, Equation 20 predicts that a plot of σ_R against D_R should be linear with slope σ_T and intercept T.

The result of a strength-theory analysis applied to our experimental results is shown in Fig. 6. The master-curve analysis shows the theory to be very poor.

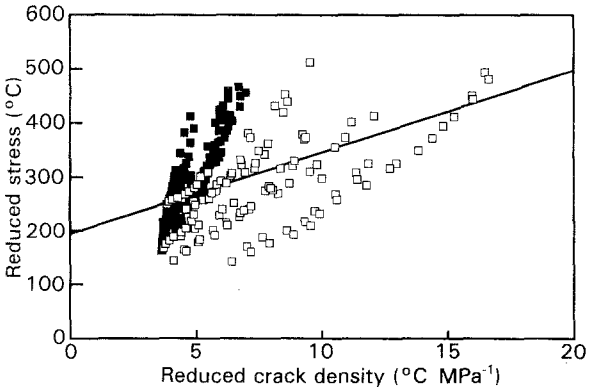

Figure 6 A master-curve analysis of all AS4/3501-6 laminates using a maximum-stress failure criterion and a one-dimensional stress analysis: (□) $[0_n/90_m]_s$ and (■) $[90_n/0_m]_s$. Data for crack densities less than 0.3 mm^{-1} are not included in this plot.

The results from individual laminates are somewhat non-linear and they do not overlap the results from other laminates. Furthermore, the results from $[(S)/90_n]_s$ (□) and $[90_n/(S)]_s$ (■) laminates segregate into two groups. This segregation is a characteristic of all one-dimensional analyses. Any analysis that ignores the z-dependence of the stress state will fail to make a distinction between inner and outer 90°-ply groups. We therefore conclude that no model based on a one-dimensional stress analysis can successfully predict results for both $[(S)/90_n]_s$ and $[90_n/(S)]_s$ laminates. If we draw a least-squares linear fit through the data in Fig. 6, the slope and intercept give $\sigma_T = 15.2$ MPa and $T = +192$ °C. These results are unreasonable because the transverse tensile strength of AS4/3501-6 laminates is higher than 15.2 MPa and T must be below zero for laminates that were cooled after processing.

There are two problems with the Garrett and Bailey model. First, it uses a one-dimensional, shear-lag, stress analysis. Secondly it uses a poor failure criterion. To investigate the limitations of the stress analysis, we implemented the strength model using the two-dimensional, variational analysis. This approach still gave poor results. The poor results with the more accurate stress analysis suggest that it is the use of a strength-failure criterion that is the more serious and fundamental problem with this analysis. There have been some attempts to develop more sophisticated strength models, such as probabilistic strength models [9, 13, 22, 34, 43]. These models, however, have been found to require *in situ* laminate-strength properties and therefore would also give poor master curves [30]. We suggest that strength models cannot adequately predict failure in composite laminates.

Because of the problems with all strength analyses, numerous authors have suggested energy-failure criteria for predicting microcracking [3, 5, 17, 20, 23, 25, 30, 35–37, 39, 42]. Although an energy-release-rate-failure criterion was first proposed for microcrack initiation [3, 5, 17], Caslini *et al.* [20] were the first to suggest using the total microcrack-energy-release rate to predict microcrack density as a function of applied load. They used a one-dimensional analysis that assumes parabolic displacements in the 90° plies [31, 32] to express the structural modulus as a function of crack density. They treated the crack area, $A = 2t_1 WLD$, as a continuous variable, and differentiated the modulus expression to find the energy-release rate. Because they take an analytical derivative as a function of crack area, we refer to this approach as the *analytical-derivative approach.* By treating Equation 5 as a definition of $Y(D)$, the Caslini *et al.* [20] result for G_m can be expressed using

$$Y_{1D,a}(D) = \frac{C_1}{C_3\Phi}(\tanh \Phi\rho - \Phi_\rho \operatorname{sech}^2\Phi\rho) \quad (22)$$

where the subscript "1D, a" denotes one-dimensional stress analysis and an analytical-derivative approach, and $\Phi = (3G_{xx}^{(1)}C_1)^{1/2}$. Han *et al.* [35, 36] describe a similar analysis, but used crack-close methods to calculate G_m. Because their results are identical to those of Caslini *et al.* [20], the Han *et al.* approach [35, 36] is also an analytical-derivative model. Finally, we note that the seemingly more realistic stress analysis based on the assumption of parabolic displacements in the 90° plies [31, 32, 35, 36], unfortunately only results in a trivial change in Φ by a factor of $3^{1/2}$ when compared to the simple Garrett and Bailey [1] analysis.

By replacing $Y(D)$ with $Y_{1D,a}(D)$ we can evaluate the microcracking models in [20, 35, 36]. The results of such an analysis applied to our experimental results are shown in Fig. 7. This master-curve analysis was the worst of any model we evaluated. The results from individual laminates are fairly linear but they give slopes and intercepts corresponding to toughnesses as high as 10^{12} J m^{-2} and values of T that imply specimen temperatures well below absolute zero. These are clearly unreasonable results. The least-squares linear fit through the data in Fig. 7 gives $G_{mc} = 2$ J m^{-2} and $T = 323$ °C. The global fit does not pass through the data (because the data from different laminates do not overlap) and the global-fitting constants are unrealistic.

In Section 4.3., we argued that Caslini *et al.*'s original suggestion [20] about analysing microcracking using energy-release-rate is appropriate. We are left with explaining why their energy-release-rate approach is a complete failure. Our first attempt was to

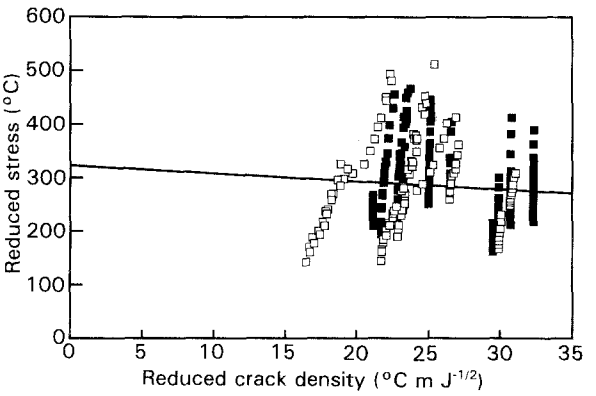

Figure 7 A master-curve analysis of all AS4/3501-6 laminates using an analytical-derivative energy-release-rate failure criterion and a one-dimensional stress analysis. Data for crack densities less than 0.3 mm^{-1} are not included in this plot. Key: as Fig. 6.

use the variational-mechanics stress analysis and to calculate G_m by a similar analytical-derivative approach. This made slight improvements in the master curve, but the overall quality and the fitting constants were still unsatisfactory. We suggest instead that the analytical-derivative approach is non-physical and therefore $Y_{1D,a}(D)$ gives the wrong energy-release rate. The analytical-derivative, energy-release rate at a given crack density corresponds to the unlikely fracture event whereby all cracks close and then reopen again as periodic cracks with a slightly higher crack density. In real microcracking, one microcrack forms between two existing microcracks. Apparently the energy-release rate for this process is dramatically different from that calculated with an analytical derivative.

Laws and Dvorak [37] were the first to suggest modelling the actual fracture process. They calculated the change in energy associated with the formation of a new microcrack between two existing microcracks. Because they model a discrete process, we call their approach the *discrete-derivative approach.* We cast Laws and Dvorak results [37] in the form of the variational analysis by redefining $Y(D)$ to be

$$Y_{1D,d}(D) = \frac{C_1}{C_3\Phi}(2\tanh f\Phi\rho/2 - \tanh f\Phi\rho) \quad (23)$$

where the subscript "1D,d" denotes one-dimensional stress analysis and a discrete-derivative approach, and f is the factor introduced earlier to account for the tendency of microcracks to prefer larger than average microcrack intervals. Following Reifsnider [2], Laws and Dvorak [37] used a shear-lag analysis that assumes an interlayer of unknown thickness and stiffness between the sublaminate (S) and the 90° plies. Their Φ can be expressed as

$$\Phi = \left(\frac{Gt_1 C_1}{t_0}\right)^{1/2} \quad (24)$$

where G is the shear modulus of the interlayer and t_0 is its thickness.

By replacing $Y(D)$ with $Y_{1D,d}(D)$ we can evaluate the Laws and Dvorak microcracking model [37]. A drawback of their analysis is that the effective stiffness of the interlayer is an unknown parameter. Laws and Dvorak [37] suggested a circular scheme in which G/t_0 is determined by prior knowledge of G_{mc} and the stress required to form the first microcrack. Because of our concern about the sensitivity of low-crack-density results to laminate-processing flaws, we used the high-crack-density results from the single laminate in Fig. 4 to determine G/t_0. We varied G/t_0 until the slope of the Laws-and-Dvorak analysis master-curve [37] gave G_{mc} equal to the variational-analysis result of $280\,J\,m^{-2}$. This exercise yielded $G/t_0 = 4000\,N\,mm^{-1}$, a linear master curve, and an intercept of $T = -73\,°C$. These initial results were promising. The results of a master-curve analysis applied to all our experimental results using $Y_{1D,d}(D)$, $G/t_0 = 4000\,N\,mm^{-1}$, and $f \approx 1.2$ are shown in Fig. 8. This master-curve analysis is the most satisfactory of all the previous literature models but it still has serious problems. Most importantly, the results from individual lamina do not overlap. As is characteristic of one-dimensional analyses, the results from $[(S)/90_n]_s$ and $[90_n/(S)]_s$ laminates segregate into two groups. The least-squares linear fit through the data in Fig. 8 gives $G_{mc} = 44\,J\,m^{-2}$ and $T = +124\,°C$. The global fit does not pass through the data (because the data from different laminates do not overlap) and the global-fitting constants are unrealistic.

We believe the only problem with the Laws and Dvorak [37] analysis is its use of an oversimplified, one dimensional stress analysis. If their failure criterion is implemented with the variational-mechanics stress analysis, the result is equivalent to the analysis first presented by Nairn [42]. As shown in Section 4.3, such an analysis gives a good master curve (see Fig. 5).

It is possible to evaluate many other theories by using master-curve analyses. One could combine any failure criterion (strength, analytical-derivative G_m, or discrete-derivative G_m) with any stress analysis (one-dimensional analyses, two-dimensional variational analyses, refined variational analysis [44], or numerical stress analyses). We tried many such combinations and found that all attempts at using one-dimensional stress analyses are complete failures. If nothing else, they always fail to differentiate between $[(S)/90_n]_s$ and $[90_n/(S)]_s$ laminates. When more accurate stress analyses, such as variational analysis, are used, all attempts at using strength or analytical-derivative G_m failure criteria are also complete failures. We finally concluded that only the specific combination of a sufficiently accurate stress analysis (e.g. variational-stress analysis) with a discrete-derivative evaluation of G_m is capable of producing a meaningful master curve.

4.5. The effect of distribution of microcrack spacings

One difficulty in analysing microcracking is the need for the f-factor to account for the effect of a distribution in crack spacings. We treated f as an adjustable parameter, but found that it is layup independent and usually $f \approx 1.2$. Fortunately, the precise choice of f has only a second-order effect on the measured value of

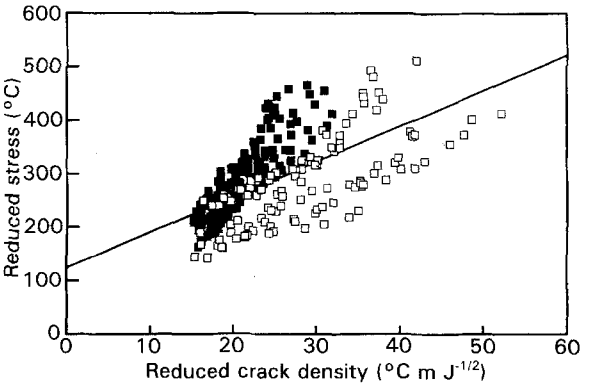

Figure 8 A master-curve analysis of all AS4/3501-6 laminates using a discrete-derivative, energy-release-rate failure criterion and a one-dimensional stress analysis. Data for crack densities less than $0.3\,mm^{-1}$ are not included in this plot. Key: as Fig. 6.

G_{mc}. When we varied f from 1.1 to 1.7, the master-curve slope gave G_{mc} values from 204 J m^{-2} to 333 J m^{-2} or $G_{mc} \approx 270 \pm 70$ J m^{-2}. Thus, the microcracking toughness of any material can be reasonably characterized without being concerned with detailed knowledge of the f-factor. For more precise work, however, measuring f may be warranted. In this section we describe one technique for measuring f. When successful, this technique supports the claim that the f-parameter has physical meaning and is not merely an adjustable fitting parameter.

In principle, the need for f can be avoided by directly measuring $Y(D)$. By Equation 6 or 12 we could plot $D\langle\chi(\rho)\rangle$ or $D\langle\chi_a(\rho)\rangle$ as a function of D and numerically differentiate it to measure $Y(D)$ or $Y_a(D)$. We tried this approach and found that the inherent difficulties in numerically differentiating fracture data made it an impractical approach. To avoid the differentiation step, we developed an integral approach. We treated Equations 8 and 13 as single-parameter representations of $Y(D)$. Inserting $Y(D)$ in Equation 8 into $Y(D)$ in Equation 6 gives

$$\frac{d\langle\chi(\rho)\rangle}{dD} = \frac{2\chi(f\langle\rho\rangle/2) - \chi(f\langle\rho\rangle) - \langle\chi(\rho)\rangle}{D} \tag{25}$$

This first-order differential equation can easily be integrated to predict $\langle\chi(\rho)\rangle$ as a function of D for any value of f. By comparing the prediction to experimental results it is possible to measure f. An advantage over the direct measurement of $Y(D)$ is that the experimental determination of $\langle\chi(\rho)\rangle$ does not require any numerical differentiation. A similar treatment can also be applied to $[90_n/(S)]_s$ laminates using $Y_a(D)$ and $\chi_a(\rho)$ along with Equations 13 and 12.

In brief, when each test was periodically stopped to find the crack density, we also did the tedious task of measuring the complete distribution of crack spacings. From $\rho_1, \rho_2, \ldots, \rho_N$ at each crack density, we calculated $\langle\chi(\rho)\rangle$ as a function of D. In a simple computer program, we varied f until the predicted $\langle\chi(\rho)\rangle$ agreed with the measured $\langle\chi(\rho)\rangle$. Some typical results are given in Fig. 9. The symbols are experimental points and the three smooth lines are predictions for $f = 1.00$, $f = 1.25$, and $f = 1.50$. At low crack densities $\langle\chi(\rho)\rangle$ is constant and the predictions are independent of f. Therefore, the low-crack-density data cannot be used to measure f. At higher crack density, $\langle\chi(\rho)\rangle$ begins to decrease. The onset and the rate of decrease are sensitive functions of f. For the laminate in Fig. 9, a value of $f = 1.25$ predicted the complete experimental curve. This result suggests that the single-parameter representation of $Y(D)$ is reasonable and accurate. If it were not, a single value of f could not predict the results. The curves for $f = 1.00$ and $f = 1.50$ illustrate the precision in measuring f. There is enough sensitivity in the high crack density to estimate the precision in f for this laminate as $f = 1.25 \pm 0.05$.

We did the measurement shown in Fig. 9 for each laminate in this study and got good results for most $[(S)/90_n]_s$ laminates. The measured f values ranged from 1.15 to 1.35. These values agreed well with the

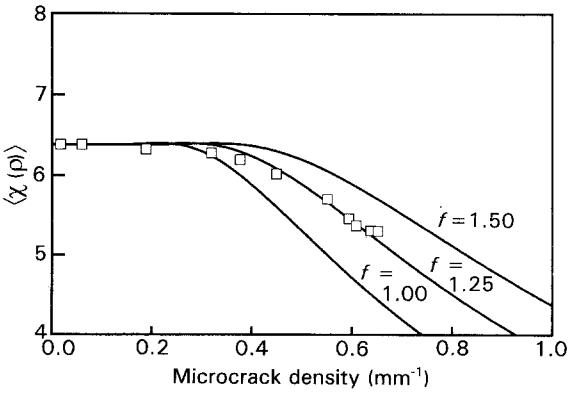

Figure 9 (□) The measured value of $\langle\chi(\rho)\rangle$ and (——) the predicted value of $\langle\chi(\rho)\rangle$ for a $[0/90_4]_s$ laminate. The three prediction lines are for $f = 1.00$, $f = 1.25$ and $f = 1.50$. The best prediction of the experimental results was when $f = 1.25$.

value of $f \approx 1.2$ that was previously determined by fitting theory to raw data with f as an adjustable parameter (see Fig. 2). For some $[(S)/90_n]_s$ laminates the experimental results only included low-crack-density data. As shown in Fig. 9, the low-crack-density results are insensitive to f and thus the data from these laminates could not be used to measure f. Our attempts to measure f in $[90_n/(S)]_s$ laminates were less successful. We could predict the onset and the rate of the decrease in $\langle\chi_a(\rho)\rangle$ at high crack density, but the predictions required selecting $f = 1.45$ to 1.9. These values are inconsistent with fits of theory to raw data that treat f as an adjustable parameter. We do not know the reasons for our inability to measure f in $[90_n/(S)]_s$ laminates. It is possible that our measurement of $\langle\chi_a(\rho)\rangle$ was oversimplified. By averaging $\chi_a(\rho)$, we were implicitly assuming that there is perfect stagger. In other words, we assume that all crack intervals appeared as in Fig. 3b where the microcrack in one 90°-ply groups is exactly centred between two microcracks in the other 90°-ply group. A more precise calculation of $\langle\chi_a(\rho)\rangle$ that accounts for imperfect stagger might result in better f values.

5. Discussion and conclusions

It is relatively easy to fit approximate theories to experimental results from one or two laminates, which is what many researchers do. When theories are required to simultaneously fit results from 18 different laminates, however, the task is much harder. Our large data base thus allowed us to make critical evaluations of various microcracking theories. We found that of the existing theories, only an energy-based failure criterion (implemented using a discrete evaluation of the energy-release rate) and a two-dimensional variational-stress analysis were capable of analysing all the results. The differences between various theories were best visualized using master-curve analyses. Those master-curves showed that the differences between the theories are not subtle. All attempts at using one-dimensional stress analyses, regardless of the failure criterion, were very poor. Even the more accurate variational-stress analysis gave poor results when it

was used to predict failure with an inappropriate failure criterion. The variational-stress analysis and discrete-energy-release-rate method we recommended can be viewed as not only the best model but also as the only acceptable model. Of course, additional models that build on the recommended approach while refining the variational analysis [44] would also produce acceptable results.

A crucial aspect of any microcracking theory is the failure criterion used to generate the predictions. We tried many failure criteria and found that only a fracture mechanics failure criterion based on the actual fracture process provided a fundamental interpretation of all results. The fracture mechanics criterion states that microcracking occurs when the energy-release rate associated with the formation of the next microcrack exceeds the microcracking toughness of the material. It is important that the calculated energy-release rate corresponds to the actual fracture process. For microcracking this involves modeling the fracture event of a new microcrack forming between two existing microcracks. One approach that ignores the actual fracture process is to treat crack density as a continuous variable and analytically differentiate the strain energy to get a pseudo-energy-release rate. This analytical-derivative approach ignores the actual fracture process and does not agree with experimental results.

Maximum-stress or maximum-strain failure criteria were particularly bad. Our results substantiate this conclusion for microcracking experiments, but the conclusion is probably more general. We suggest that simple maximum stress or even more sophisticated quadratic failure criteria are not based on the energy principles of fracture mechanics, and have no fundamental physical basis, and therefore should not be expected to give useful predictions about any composite failure mode. For example, many laminated-plate analyses predict the onset of failure using first-ply failure criteria that are based on simple maximum stress rules. The initiation of microcracking in this paper can be viewed as an experimental study on first-ply failure. The inability of strength models to make useful predictions about our experimental results is verification that first-ply failure models are inappropriate. If first-ply failure models are inappropriate, we further suggest that more complicated composite-failure theories that are rooted in simple strength rules are equally inappropriate.

We found that a good failure criterion alone is not sufficient to develop a successful analysis of microcracking. The failure criterion must be used in conjunction with some stress analysis before it can make predictions. That stress analysis must be sufficiently accurate to ensure good results. We found, for example, that the qualitative stresses calculated by one-dimensional stress analyses always gave poor results. The results were poor even when coupled with the best failure criterion such as in the model of Laws and Dvorak [37]. In contrast, the more accurate two-dimensional, variational-stress analysis coupled with the best failure criterion gave good results. If one plots the stresses calculated by a one-dimensional analysis and those calculated by a variational analysis, the differences are marked, but they are hardly dramatic [30]. We were thus initially surprised by the dramatic differences between the predictions based on the two analyses. A qualitative interpretation of the differences can follow from realizing that fracture is an instability event. When calculating instability processes, minor differences in input stresses can lead to dramatic differences in predictions. In other words, the increased accuracy in the stresses attributed to the variational analysis was crucial to the predictions of microcracking.

The master-curve analysis in Fig. 5 provides a new technique for measuring a useful material property – the microcracking or *intralaminar* toughness of a composite material. Although it is truly a measured property, the numerical accuracy of G_{mc} depends on the accuracy of G_m in Equations 5 and 11. To verify the measured G_{mc} using independent experiments, we measured the *transverse* fracture toughness of unidirectional AS4/3501-6 laminates. By transverse toughness we mean the material toughness for a crack running parallel to the fibres, but normal to the plies. In other words, the propagation of an *intralaminar* crack. The transverse toughness was measured using a conventional double-cantilever beam for delamination specimens and rotating it by 90° so that the previously *interlaminar* crack becomes an *intralaminar* crack. The results were analysed using the DCB specimen analysis recommended by Hashemi *et al.* [45]. The resulting transverse toughness was $G_{tc} = 309\ J\,m^{-2}$ which is close to $G_{mc} = 279\ J\,m^{-2}$, determined in Fig. 5. It is noteworthy that both G_{mc} and G_{tc} are significantly higher than the delamination fracture toughness which is $G_{Ic} = 175\ J\,m^{-2}$ [46]. Experience with other material systems shows that G_{mc} is usually similar to G_{Ic}. Closer inspection, however, reveals that G_{Ic} can be significantly less or significantly greater than G_{mc} depending on structural and material variables [30].

There are three practical details worthy of discussion. First the intercept of the master curve in Equation 14 is T which defines the *effective* level of residual stress in the specimen. In principle, a master-curve analysis of microcracking experiments provides a measure of both G_{mc} and of the level of residual thermal stresses. The results in Figs 4 and 5 show that residual stresses can be reliably measured. When the results from individual laminates are considered separately, however, the resulting measurement of T is sensitive to small experimental scatter. For the 18 laminates in this study, individual master curves gave T ranging from -33 to $-297\,°C$. The master-curve analysis can thus not be recommended as an accurate way to measure residual stresses. For the most accurate determination of G_{mc}, we recommend measuring T and plotting a modified reduced stress, instead,

$$\sigma_R = -\frac{k_m^{(1)}}{k_{th}^{(1)}}\sigma_0 - T \tag{26}$$

against reduced crack density. The resulting plot should be linear and should pass through the origin

with a slope of $(G_{mc})^{1/2}$. Fits of such master curves that are forced to pass through the origin can give greater precision in G_{mc} and smaller laminate-to-laminate variability in the measured G_{mc}. This approach has the side-benefit of producing master curves for laminates with real variations in T that would otherwise not fall on a single master curve.

Following the suggestion of Liu and Nairn [23], we assumed that low-crack-density results were dominated by specimen flaws and should be eliminated from the master-curve analysis when measuring the material toughness. The second point to discuss is whether the decisions regarding which points to eliminate influenced the results. The low-crack-density points are relatively few in number and are all clustered around the same reduced crack density (see Fig. 4). Fortunately the global fit to all experimental points is nearly unaffected by inclusion or elimination of the low-crack-density results. For the most accurate results we recommend eliminating them. It is easy to decide which points should be eliminated by determining which low-crack-density points deviate from the predicted-master-curve line.

The third point is the undetermined f-factor. Our experiments on $\langle \chi(\rho) \rangle$ show that f is not a fudge factor to produce better fits, but rather a meaningful physical constant. The use of an f-factor is an approximate method that accounts for the effect of variations in microcrack spacings which occur in all real laminates. Without the f-factor, the analysis would be insensitive to variations in microcrack spacings, and would thus be incapable of predicting their effect on fracture properties. The f-factor, therefore, should not be viewed as a limitation of the variational-analysis model, but rather as a manifestation of its ability to include crack-spacing-variation effects. Furthermore, one should question the validity of any microcracking analysis that does not include a similar factor or does not include some method for dealing with variations in crack spacings.

Acknowledgements

This work was supported in part by a contract from NASA Langley Research Center (NAS1-18833) monitored by Dr John Crews, in part by a gift from ICI Advanced Composites monitored by Dr J. A. Barnes, and in part by a gift from the Fibers Department of E. I. duPont deNemours and Company monitored by Dr Alan R. Wedgewood.

References

1. K. W. GARRETT and J. E. BAILEY, *J. Maters: Sci.* **12** (1977) 157.
2. K. L. REIFSNIDER, Proceedings of the Fourteenth Annual Meeting of SES, Lehigh, PA, November, (1977) p. 373.
3. A. PARVIZI, K. W. GARRETT and J. E. BAILEY, *J. Mater. Sci.* **13** (1978) 195.
4. A. PARVIZI and J. E. BAILEY, *J. Mater. Sci.* **13** (1978) 2131.
5. J. E. BAILEY, P. T. CURTIS and A. PARVIZI, *Proc. R. Soc. Lond. A* **366** (1979) 599.
6. M. G. BADER, J. E. BAILEY, P. T. CURTIS and A. PARVIZI, Proceedings of the Third International Conference on Mechanical Behavior of Materials, Cambridge, England, 1979, **3** (1979) 227.
7. F. W. CROSSMAN, W. J. WARREN, A. S. D. WANG and G. E. LAW Jr, *J. Comp. Mater. Suppl.* **14** (1980) 89.
8. W. W. STINCHCOMB, K. L. REIFSNIDER, P. YEUNG and J. MASTERS, *ASTM STP* **723** (1981) 64.
9. D. L. FLAGGS and M. H. KURAL, *J. Comp. Mater.* **16** (1982) 103.
10. F. W. CROSSMAN and A. S. D. WANG, *ASTM STP* **775** (1982) 118.
11. A. L. HIGHSMITH and K. L. REIFSNIDER, *ASTM STP* **775** (1982) 103.
12. P. W. MANDERS, T. W. CHOU, F. R. JONES and J. W. ROCK, *J. Mater. Sci.* **19** (1983) 2876.
13. P. W. M. PETERS, *J. Comp. Mater.* **18** (1984) 545.
14. R. JAMISON, K. SCHULTE, K. L. REIFSNIDER and W. W. STINCHCOMB, *ASTM STP* **836** (1984) 21.
15. A. S. D. WANG, P. C. CHOU and S. C. LEI, *J. Comp. Mater.* **18** (1984) 239.
16. A. S. D. WANG, *Comp. Tech. Rev.* **6** (1984) 45.
17. A. S. D. WANG, N. N. KISHORE and C. A. LI, *Comp. Sci. Tech.* **24** (1985) 1.
18. M. G. BADER and LYNN BONIFACE, Proc. 5th Int'l Conf. on Comp. Mat. (Met. Soc., San Diego, CA, July 1985) p. 221.
19. L. BONIFACE, P. A. SMITH, S. L. OGIN and M. G. BADER, Proc 6th Int'l Conf. on Comp. Mat. **3** (1987) p. 156.
20. M. CASLINI, C. ZANOTTI and T. K. O'BRIEN, *J. Comp. Tech. Research*, Winter (1987) 121. (Also appeared as NASA TM89007, 1986).
21. S. E. GROVES, C. E. HARRIS, A. L. HIGHSMITH and R. G. NORVELL, *Experimental Mechanics* March (1987) 73.
22. K. C. JEN and C. T. SUN, Proc. of the Amer. Soc. Comp, 5th Tech. Conf. (Technomi 2, E. Lausing, MI, June 1990) p. 350.
23. S. LIU and J. A. NAIRN, *J. Reinf. Plast. Comp.* **11** (1992) 158.
24. S. YALVAC, L. D. YATS and D. G. WETTERS, *J. Comp. Mater.* (1992), in press.
25. J. A. NAIRN and S. HU, *Engng Fract. Mech.* **41** (1992) 203.
26. D. S. ADAMS and C. T. HERAKOVICH, *J. Thermal Stresses* **7** (1984) 91.
27. D. E. BOWLES, *J. Comp. Mater.* **17** (1984) 173.
28. J. A. NAIRN and S. HU, *Int. J. Fract.* (1992) in press.
29. S. HU, J. S. BARK and J. A. NAIRN, *Comp. Sci. Tech.* (1992) submitted.
30. J. A. NAIRN and S. HU, in "Damage mechanics of composite materials," edited by R. Talreja (Elsevier Science Publishers, Barking, UK, 1992) in press.
31. S. L. OGIN, P. A. SMITH and P. W. R. BEAUMONT, *Comp. Sci. Tech.* **22** (1985) 23.
32. S. L. OGIN, P. A. SMITH and P. W. R. BEAUMONT, *Comp. Sci. Tech.* **24** (1985) 47.
33. D. L. FLAGGS, *J. Comp. Mater.* **19** (1985) 29.
34. H. FUKUNAGA, T. W. CHOU, P. W. M. PETERS and K. SCHULTE, *J. Comp. Mater.* **18** (1984) 339.
35. Y. M. HAN, H. T. HAHN, and R. B. CROMAN, Proc. Amer. Soc. of Comp., 2nd Tech. Conf. (Technomi 2, Newark, DE, Sept. 1987) 503.
36. Y. M. HAN, H. T. HAHN and R. B. CROMAN, *Comp. Sci. Tech.* **31** (1987) 165.
37. N. LAWS and G. J. DVORAK, *J. Comp. Mater.* **22** (1988) 900.
38. R. J. NUISMER and S. C. TAN, *J. Comp. Mater.* **22** (1988) 306.
39. S. C. TAN and R. J. NUISMER, *J. Comp. Mater.* **23** (1989) 1029.
40. Z. HASHIN, *Mech. of Mater.* **4** (1985) 121.
41. Z. HASHIN, *Engng Fract. Mech.* **25** (1986) 771.
42. J. A. NAIRN, *J. Comp. Mater.* **23** (1989) 1106. (See *errata: J. Comp. Mater.* **24** (1990) 233.)
43. H. FUKUNAGA, T. W. CHOU, K. SCHULTE and P. W. M. PETERS, *J. Mater. Sci.* **19** (1984) 3546.
44. J. VARNA and L. BERGLUND, *J. Comp. Tech. Res.* **13** (1991) 97.
45. S. HASHEMI, A. J. KINLOCH and J. G. WILLIAMS, *Proc. R. Soc. Lond. A* **347** (1990) 173.
46. D. L. HUNSTON, *Comp. Tech. Rev.* **6** (1984) 176.

Received 23 April 1992
and accepted 24 February 1993

Appendix

In the variational-mechanics analysis of $[(S)/90_n]_s$ laminates [40, 41, 23, 42] we define the following constants:

$$C_1 = \frac{1}{E_x^{(1)}} + \frac{1}{\lambda E_x^{(2)}} \tag{27}$$

$$C_2 = \frac{\nu_{xx}^{(1)}}{E_x^{(1)}}(\lambda + \tfrac{2}{3}) - \frac{\lambda \nu_{xx}^{(2)}}{3E_x^{(2)}} \tag{28}$$

$$C_3 = \frac{1}{60E_x^{(1)}}(15\lambda^2 + 20\lambda + 8) + \frac{\lambda^3}{20E_x^{(2)}} \tag{29}$$

$$C_4 = \frac{1}{3G_{xx}^{(1)}} + \frac{\lambda}{3G_{xx}^{(2)}} \tag{30}$$

where $E_x^{(i)}$ and $E_z^{(i)}$ are the x- and z-direction moduli of ply-group i, $G_{xx}^{(i)}$ is the (x, z)-plane shear modulus of ply-group i, and $\lambda = t_1/t_2$. Superscripts "(1)" and "(2)" denote properties of the 90° plies and the (S) sublaminate, respectively. t_1 and t_2 are the ply thicknesses defined in Fig. 3. Defining $p = (C_2 - C_4)/C_3$ and $q = C_1/C_3$ there are two forms for the function $\phi(\xi)$ in Equation 1. When $4q/p^2 > 1$

$$\begin{aligned}\phi(\xi) = {} & \frac{2(\beta \sinh \alpha\rho \cos \beta\rho + \alpha \cosh \alpha\rho \sin \beta\rho)}{\beta \sinh 2\alpha\rho + \alpha \sin 2\beta\rho} \\ & \times \cosh \alpha\xi \cos \beta\xi \\ & + \frac{2(\beta \cosh \alpha\rho \sin \beta\rho - \alpha \sinh \alpha\rho \cos \beta\rho)}{\beta \sinh 2\alpha\rho + \alpha \sin 2\beta\rho} \\ & \times \sinh \alpha\xi \sin \beta\xi\end{aligned} \tag{31}$$

where

$$\alpha = \tfrac{1}{2}(2q^{1/2} - p)^{1/2}, \quad \beta = \tfrac{1}{2}(2q^{1/2} + p)^{1/2} \tag{32}$$

When $4q/p^2 < 1$

$$\begin{aligned}\phi(\xi) = {} & \frac{\tanh \alpha\rho \tanh \beta\rho}{\beta \tanh \beta\rho - \alpha \tanh \alpha\rho} \\ & \times \left[\frac{\beta \cosh \alpha\xi}{\sinh \alpha\rho} - \frac{\alpha \cosh \beta\xi}{\sinh \beta\rho}\right]\end{aligned} \tag{33}$$

where

$$\begin{aligned}\alpha &= \left[-\frac{p}{2} + \left(\frac{p^2}{4} - q\right)^{1/2}\right]^{1/2}, \\ \beta &= \left[-\frac{p}{2} + \left(\frac{p^2}{4} - q\right)^{1/2}\right]^{1/2}\end{aligned} \tag{34}$$

The function $\chi(\rho)$ used in defining the energy-release rate for microcracking in $[(S)/90_n]_s$ laminates also has two forms. When $4q/p^2 > 1$

$$\chi(\rho) = 2\alpha\beta(\alpha^2 + \beta^2)\frac{\cosh 2\alpha\rho - \cos 2\beta\rho}{\beta \sinh 2\alpha\rho - \alpha \sin 2\beta\rho} \tag{35}$$

When $4q/p^2 < 1$

$$\chi(\rho) = \alpha\beta(\beta^2 - \alpha^2)\frac{\tanh \alpha\rho \tanh \beta\rho}{\beta \tanh \beta\rho - \alpha \tanh \alpha\rho} \tag{36}$$

In the variational-mechanics analysis of $[90_n/(S)]_s$ laminates [25] we define some new constants:

$$C_{2a} = -\frac{\nu_{xx}^{(1)}}{3E_x^{(1)}} + \frac{\nu_{xx}^{(2)}}{E_x^{(2)}}\left(1 + \frac{2\lambda}{3}\right) \tag{37}$$

$$C_{3a} = \frac{1}{20E_z^{(1)}} + \frac{\lambda}{60E_z^{(2)}}(8\lambda^2 + 20\lambda + 15) \tag{38}$$

$$C_1^* = \frac{1}{E_x^{(1)}} + \frac{(1 + 2\lambda)^2}{\lambda^3 E_x^{(2)}} \tag{39}$$

$$C_2^* = -\frac{\nu_{xx}^{(1)}}{3E_x^{(1)}} + \frac{\nu_{xx}^{(2)}}{E_x^{(2)}}\left[\frac{(1 + 2\lambda)(2 + \lambda)}{3\lambda}\right] \tag{40}$$

$$C_3^* = \frac{1}{20E_z^{(1)}} + \frac{\lambda}{60E_z^{(2)}}(2\lambda^2 + 7\lambda + 8) \tag{41}$$

$$C_4^* = \frac{1}{3G_{xx}^{(1)}} + \frac{1 + \lambda + \lambda^2}{3\lambda G_{xx}^{(2)}} \tag{42}$$

The function $\phi_a(\xi)$ that defines the stresses in the 90° plies is expressed in terms of two new functions

$$\phi_a(\xi) = \begin{cases} X_0(\xi) + Y_0(\xi) & \text{if } |\xi| < \rho/2 \\ X_0(\xi) - Y_0(\xi) & \text{if } \rho/2 < |\xi| < \rho \end{cases} \tag{43}$$

Redefining $p = (C_{2a} - C_4)/C_{3a}$ and $q = C_1/C_{3a}$ there are two forms for the function X_0. When $4q/p^2 > 1$

$$\begin{aligned}X_0(\xi) = {} & \frac{C_3^* \chi^*(\tfrac{1}{2}\rho)}{C_{3a}\chi(\tfrac{1}{2}\rho) + C_3^* \chi^*(\tfrac{1}{2}\rho)} \\ & \times \left[\cosh \alpha\xi \cos \beta\xi - \frac{\alpha \sinh \alpha\rho - \beta \sin \beta\rho}{\beta \sinh \alpha\rho + \alpha \sin \beta\rho}\right. \\ & \times \sinh \alpha\xi \sin \beta\xi + \frac{\cosh \alpha\rho - \cos \beta\rho}{\beta \sinh \alpha\rho + \alpha \sin \beta\rho} \\ & \left. \times (\alpha \cosh \alpha\xi \sin \beta\xi - \beta \sinh \alpha\xi \cos \beta\xi)\right]\end{aligned} \tag{44}$$

When $4q/p^2 < 1$

$$\begin{aligned}X_0(\xi) = {} & \frac{C_3^* \chi^*(\tfrac{1}{2}\rho)}{C_{3a}\chi(\tfrac{1}{2}\rho) + C_3^* \chi^*(\tfrac{1}{2}\rho)} \\ & \times \frac{1}{\beta \tanh \beta\rho/2 - \alpha \tanh \alpha\rho/2} \\ & \times [\beta \tanh \beta\rho/2 \cosh \alpha\xi - \alpha \tanh \alpha\rho/2 \cosh \beta\xi \\ & + \tanh \alpha\rho/2 \tanh \beta\rho/2 (\alpha \sinh \beta\xi - \beta \sinh \alpha\xi)]\end{aligned} \tag{45}$$

In Equations 44 and 45, α, β, and $\chi(\rho)$ are the same as in Equations 32–36 except that the redefined forms of p and q are used. The function $\chi^*(\rho)$ is defined below. For the function $Y_0(\xi)$ we define $p^* = (C_2^* - C_4^*)/C_3^*$ and $q^* = C_1^*/C_3^*$. When $4q^*/(p^*)^2 > 1$

$$\begin{aligned}Y_0(\xi) = {} & -\frac{C_{3a}\chi(\rho/2)}{C_{3a}\chi(\rho/2) + C_3^* \chi^*(\rho/2)} \\ & \times \left[\cosh \alpha^*\xi \cos \beta^*\xi - \frac{\alpha^* \sinh \alpha^*\rho + \beta^* \sin \beta^*\rho}{\beta^* \sinh \alpha^*\rho - \alpha^* \sin \beta^*\rho}\right. \\ & \times \sinh \alpha^*\xi \sin \beta^*\xi + \frac{\cosh \alpha^*\rho + \cos \beta^*\rho}{\beta^* \sinh \alpha^*\rho - \alpha^* \sin \beta^*\rho} \\ & \left. \times (\alpha^* \cosh \alpha^*\xi \sin \beta^*\xi - \beta^* \sinh \alpha^*\xi \cos \beta^*\xi)\right]\end{aligned} \tag{46}$$

When $4q^*/(p^*)^2 < 1$

$$Y_0(\xi) = -\frac{C_{3a}\chi(\rho/2)}{C_{3a}\chi(\rho/2) + C_3^* \chi^*(\rho/2)}$$

$$\times \frac{1}{\beta^* \tanh \alpha^* \rho/2 - \alpha^* \tanh \beta^* \rho/2}$$

$$\times [\beta^* \tanh \alpha^* \rho/2 \cosh \alpha^* \xi - \alpha^* \tanh \beta\rho/2 \cosh \beta^* \xi + \alpha^* \sinh \beta^* \xi - \beta^* \sinh \alpha^* \xi] \quad (47)$$

The new function $\chi^*(\rho)$ used in the definitions of $X_0(\xi)$ and $Y_0(\xi)$ also has two forms. When $4q^*/(p^*)^2 > 1$

$$\chi^*(\rho) = 2\alpha^*\beta^*[(\alpha^*)^2 + (\beta^*)^2] \times \frac{\cosh 2\alpha^* \rho + \cos 2\beta^* \rho}{\beta^* \sinh 2\alpha^* \rho - \alpha^* \sin 2\beta^* \rho} \quad (48)$$

When $4q^*/(p^*)^2 < 1$

$$\chi^*(\rho) = \alpha^*\beta^*[(\beta^*)^2 - (\alpha^*)^2] \times \frac{1}{\beta^* \tanh \alpha^* \rho - \alpha^* \tanh \beta^* \rho} \quad (49)$$

In the previous four equations, α^* and β^* are given by Equation 32 or 34 with p and q replaced by p^* and q^*.

Finally, the function $\chi_a(\rho)$ used in defining the energy-release rate for microcracking in $[90_n/(S)]_s$ is expressed in terms of $\chi(\rho)$ and $\chi^*(\rho)$ as

$$\chi_a(\rho) = \frac{2\chi(\rho/2)}{1 + C_{3a}\chi(\rho/2)/C_3^*\chi^*(\rho/2)} \quad (50)$$